LANGMUIR

pubs.acs.org/Langmuir Article

Distinctive Adsorption Mechanism and Kinetics of Immunoglobulin G on a Nanoscale Polymer Surface

David H. Cho, Tian Xie, Patrick J. Mulcahey, Noah P. Kelleher, and Jong-in Hahm*

Cite This: *Langmuir* 2022, 38, 1458−1470 Read Online

ACCESS | Metrics & More | Article Recommendations | Supporting Information

ABSTRACT: Elucidation of protein adsorption beyond simple polymer surfaces to those presenting greater chemical complexity and nanoscopic features is critical to developing well-controlled nanobiomaterials and nanobiosensors. In this study, we repeatedly and faithfully track individual proteins on the same nanodomain areas of a block copolymer (BCP) surface and monitor the adsorption and assembly behavior of a model protein, immunoglobulin G (IgG), over time into a tight surface-packed structure. With discrete protein adsorption events unambiguously visualized at the biomolecular level, the detailed assembly and packing states of IgG on the BCP nanodomain surface are subsequently correlated to various regimes of IgG adsorption kinetic plots. Intriguing features, entirely different from those observed from macroscopic homopolymer templates, are identified from the IgG adsorption isotherms on the nanoscale, chemically varying BCP surface. They include the presence of two Langmuir-like adsorption segments and a nonmonotonic regime in the adsorption plot. Via correlation to time-corresponding topographic data, the unique isotherm features are explained with single biomolecule level details of the IgG adsorption pathway on the BCP. This work not only provides much needed, direct experimental evidence for time-resolved, single protein level, adsorption events on nanoscale polymer surfaces but also signifies mutual linking between specific topographic states of protein adsorption and assembly to particular segments of adsorption isotherms. From the fundamental research viewpoint, the correlative ability to examine the nanoscopic surface organizations of individual proteins and their local as well as global adsorption kinetic profiles will be highly valuable for accurately determining protein assembly mechanisms and interpreting protein adsorption kinetics on nanoscale surfaces. Application-wise, such knowledge will also be important for fundamentally guiding the design and development of biomaterials and biomedical devices that exploit nanoscale polymer architectures.

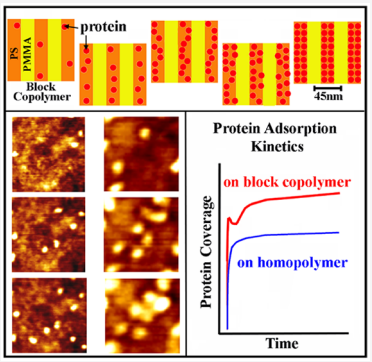

INTRODUCTION

Understanding protein adsorption to polymer surfaces is of paramount importance because the ubiquitous phenomenon of protein adsorption onto solid surfaces governs a wide range of protein mediated processes in biomaterials, biosensors, implant devices, tissue engineering, and food packaging.[1−8] In recent years, polymeric surfaces in these applications have become increasingly sophisticated, often containing nanoscale topological and chemical features to facilitate high miniaturization and functional versatility of biomaterials and biosensor devices.[9−16] In particular, block copolymers (BCPs) have shown growing relevance and utility in biomedical and biological applications.[9,10,15,16] BCPs can be thermodynamically or kinetically controlled to produce periodically arranged, nanoscale patterns of controlled sizes and shapes via self-assembly.[17−22] The resulting surfaces of BCP nanodomains, conveniently produced after a self-driven phase separation process of the BCP blocks, can be exploited as nanotemplates to effectively organize proteins in a well-controlled manner for various biomedical applications.[13,23−25] Therefore, it is critical to understand protein adsorption pathways and kinetics on the chemically varying BCP nanodomain surfaces whose characteristic feature sizes on the surface are at the length scale commensurate to the dimensions of individual proteins.

We have made research efforts in this regard.[12,13,26−28] For example, we have shown that globular proteins such as immunoglobulin G (IgG), serum albumin (SA), and horseradish peroxidase (HRP) exclusively adsorb onto the polystyrene (PS) nanodomain regions, leaving the neighboring poly(methyl methacrylate) (PMMA) nanodomain areas completely free of proteins on the BCP surface of PS-*block*-PMMA (PS-*b*-PMMA).[26,27,29,30] The highly selective adsorption of the globular proteins to PS over PMMA observed on the nanoscale BCP surface is distinct from their behaviors onto chemically homogeneous, bulk, or macroscopic scale polymer surfaces.[29,31] For example, when homopolymer surfaces of PS

Received: October 11, 2021
Revised: December 30, 2021
Published: January 17, 2022

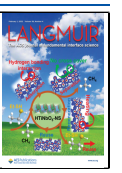

https://doi.org/10.1021/acs.langmuir.1c02710
Langmuir 2022, 38, 1458−1470

and PMMA were used instead, the proteins were found to adsorb not only on PS but also on PMMA.[29]

However, such previous research efforts on nanoscale protein adsorption have been largely centered on static instead of time-dependent adsorption behaviors.[24,26,32,33] Experimental challenges in attaining direct experimental evidence of nanoscale protein adsorption events simultaneously with their associated adsorption kinetics remain a major hurdle, especially for the very early adsorption stages, i.e. protein surface coverage well below monolayer saturation. Although many postulations currently exist in the literature for explaining protein adsorption mechanisms and pathways, they had to be deduced from bulk protein behaviors observed on macroscopic, chemically uniform surfaces.[5,23,34−36] Once again, this was largely due to the lack of direct experimental data rendering protein adsorption on nanoscale surfaces at the single biomolecular level.[1,5,6]

Our earlier findings caution us that ensemble-averaged protein adsorption behaviors can vastly differ from those of individual proteins.[27,29,31,32] Studies carried out by our and other groups also inform us that many assumed biomolecular depictions of protein adsorption from already existing mechanisms may not always accurately represent the exact details of individual protein adsorption and surface packing phenomena on nanoscale polymer surfaces.[23,33,37−41] Virtually no theoretical or computational models exist to date that explain protein adsorption mechanisms and kinetics on chemically varying BCP nanodomains. Hence, correlated topographic and kinetic experimental data directly acquired at the single biomolecule level will be highly valuable not only for verifying commonly postulated mechanisms in existing protein adsorption models but also for developing new protein adsorption mechanisms best suited for nanoscale, chemically varying BCP surfaces. Considering this, time-dependent protein adsorption studies that can provide definitive experimental evidence of nanoscale protein adsorption and surface assembly processes step by step will be immensely valuable.

Truly nanoscopic measurements of protein adsorption pathways and kinetics will require an exquisite level of spatial resolution such that both the individual proteins and the discrete polymeric nanodomains of the BCP surfaces can be discerned. Atomic force microscopy (AFM) can offer the required detection capabilities and further be exploited to correlate spatial and temporal evidence of discrete protein adsorption and assembly events as a function of time.[37,38,42−50] Electron microscopy (EM)-based approaches may provide high spatial resolution comparable to AFM,[51−55] but the requirements for staining, conductive metal coating, and high vacuum/ultralow temperature operation[51,52,56] make time-dependent protein tracking on a surface unattainable. Protein adsorption kinetics have also been studied by techniques such as infrared spectroscopy, X-ray photoelectron spectroscopy, ellipsometry, fluorescence microscopy, and optical waveguide lightmode spectroscopy.[1,2,13,31,34,57−64] However, the optical and surface sensitive techniques can be subject to labeling requirements to conjugate fluorophores, frequency-enhancing compounds, or refractive index-increasing tags.[34,61−64] In addition, a quartz crystal microbalance with dissipation monitoring (QCM-D) and surface plasmon resonance (SPR) techniques have been employed in protein adsorption studies.[63−68] The use of QCM and SPR in protein adsorption has been predominantly for investigating bulk scale protein adsorption onto chemically uniform substrates. However, no such studies are currently available in the literature that elucidate individual proteins whose adsorption yields very small amounts of proteins well below a monolayer onto particular regions of chemically varying polymer surfaces. Unlike these techniques, AFM provides sufficiently high spatial resolution for simultaneously resolving single proteins as well as the underlying, nanometer-sized polymeric features non-invasively and repeatedly.[31−33,37,38] AFM can also faithfully track particular sets of proteins on the same BCP nanodomain areas over time which, in turn, permits effective correlation of time-dependent topographic cues to pertinent protein kinetic regimes. In particular, AFM can be used to reliably obtain topological and kinetic information on protein adsorption at a very early stage when the amounts of proteins adsorbed correspond to much less than a monolayer. A thorough mechanistic and kinetic understanding of this very early adsorption stage is vital to elucidating the exact role of the underlying polymer surface in protein adsorption. This is because that the very early adsorption regime ensures that protein−polymer interactions play a dominant role in the measured adsorption kinetics, with negligible protein−protein interactions occurring between multiple protein layers. Yet, such early adsorption information cannot be readily obtained from any of the above-mentioned techniques due to limitations in spatial resolution and signal detection limit.

In this study, we undertake the experimental challenge of directly and simultaneously resolving time-dependent topographic changes and adsorption kinetic profiles. We systematically investigate IgG protein adsorption occurring onto the same PS-*b*-PMMA nanodomain areas via time-lapse AFM tracking and provide conclusive, single biomolecular level, experimental evidence of time-dependent surface assembly and packing mechanisms. Time-dependent surface coverage plots of IgG adsorption exhibit entirely different profiles on the BCP surface, i.e. a polymer surface containing nanoscale, chemically alternating BCP nanodomains, than those obtained on a homopolymer counterpart. Unlike the steadily increasing protein surface coverage over time on a PS homopolymer, the kinetic data on the BCP nanodomain surface reveals an isotherm profile with two Langmuir-like adsorption segments with an undulating curve regime. Key segments of the adsorption curves important for explaining the distinct IgG adsorption isotherm on the BCP nanodomains are identified, and each kinetic segment is substantiated by topological data revealed at the single biomolecular level. These data reveal the exact protein assembly states on the surface, including postadsorption protein rearrangement and coordinated surface packing between adjacent proteins. By correlating the local as well as more global IgG adsorption isotherms to the specific protein adsorption and assembly events taking place on the BCP surface, unique IgG adsorption pathways and associated kinetics are unambiguously revealed on the BCP nanodomain surface.

EXPERIMENTAL SECTION

Polymer substrates of PS-*b*-PMMA and PS were prepared from PS-*b*-PMMA BCP (71.4 kDa, 71% PS, a polydispersity of 1.06) and PS homopolymer (152 kDa, a polydispersity of 1.06), respectively, obtained from Polymer Source Inc. (Montreal, Canada). Silicon wafers obtained from Silicon Quest, Inc. (San Jose, CA) were cut into 1 by 1 cm^2 pieces, cleaned with ethanol, acetone, and toluene, and spun dry before coating with polymer. Ultrathin films of PS-*b*-PMMA

https://doi.org/10.1021/acs.langmuir.1c02710
Langmuir 2022, 38, 1458−1470

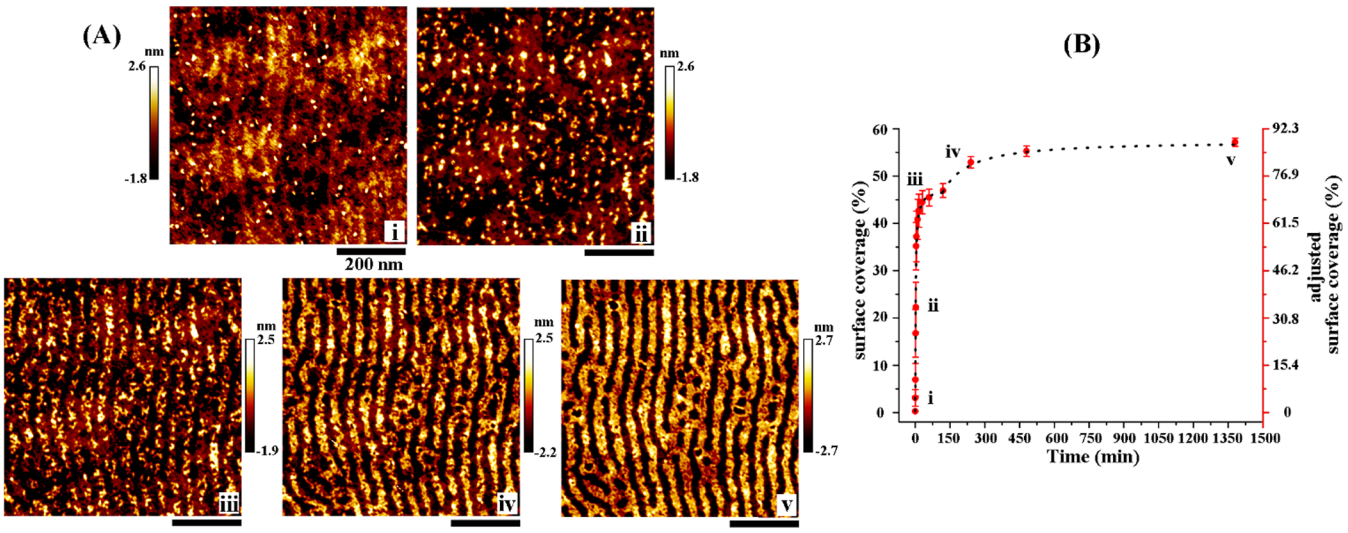

Figure 1. (A) Five representative AFM topography panels are displayed for tracking the same BCP surface of PS-*b*-PMMA to examine time-dependent IgG adsorption behaviors. The repeating stripes in the AFM images are the PS and PMMA nanodomains on the underlying BCP substrate whose nanodomain periodicity, i.e. PS to PS distance, is 45 nm. The series of AFM panels in i–v were acquired at the time points of (i) 30 s, (ii) 2.5 min, (iii) 5.5 min, (iv) 2 h, and (v) 23 h from the same BCP surface location. All scale bars shown are 200 nm in size. (B) The adsorption curve displays the surface coverage of adsorbed IgG tracked on the same surface areas of the BCP as a function of time. The left (right) vertical axis shown in percent surface coverage (adjusted percent surface coverage) indicates the percent protein surface coverage calculated with respect to the total available surface area on the BCP including the IgG-free PMMA regions (with respect to only the PS nanodomain areas). Each data point in the adsorption isotherm plot corresponds to IgG surface coverage averaged over 20 different, 2 μm × 2 μm scan areas on the BCP. The different regimes of the plot are marked i–v to aid easy correlation of the kinetic regimes with the corresponding topography panels in A.

and PS were prepared by spincasting a 2% (w/v) solution of the respective polymer in toluene onto the Si at 3500 rpm (rpm) for 1 min. Phase separation of PS-*b*-PMMA was subsequently achieved via thermal annealing in an Ar atmosphere at 240 °C for 8 h with a transient ramp-up rate of 5 °C/min and a cooling rate of 2 °C/min. This process yielded periodic stripes of alternating PS and PMMA nanodomains with a periodicity of 45 nm (PS to PS distance) at the air/polymer interface from lying-down half-cylinders exposed at the air/polymer interface. The AFM phase image of a clean, phase-separated PS-*b*-PMMA film is provided in Figure S1 in the Supporting Information to show the nanostripes on the BCP surface resulting from the alternating PS and PMMA nanodomains with a repeat spacing of 45 nm. Whole molecule bovine IgG, received from VWR Scientific Inc. (West Chester, PA) in a lyophilized form, was reconstituted in phosphate buffered saline (PBS, 10 mM mixture of Na_2HPO_4 and NaH_2PO_4, 140 mM NaCl, 3 mM KCl, pH 7.4) and further diluted to a desired protein concentration in PBS. For completing a typical series of time lapse AFM measurements, IgG deposition was repeatedly performed up to 15 times on the same BCP and PS homopolymer surfaces. For each deposition step, the polymer surface was incubated with 10 μL of 0.1 μg/mL IgG solution for various time periods in a humidity-controlled chamber, after which the sample was carefully rinsed with PBS multiple times followed by gentle drying under a stream of N_2 gas. The total time of protein adsorption corresponding to the first to the 15th deposition was 30 s, 1 min, 1.5 min, 2.5 min, 3.5 min, 10.5 min, 15.5 min, 30.5 min, 1 h, 2 h, 4 h, 8 h, 23 h, and 47 h, respectively. AFM measurements were then carried out on a MultiMode 8 AFM interfaced with a Nanoscope V controller (Bruker Corp., Santa Barbara, CA). The microscope was operated in a tapping mode at a scan rate of 1 Hz or lower in air. The measurements were conducted at room temperature under an ambient laboratory condition with a relative humidity of ~35%. Si tips (Veeco Instruments, Santa Barbara, CA) with a nominal tip radius of ~5 nm, a typical resonant frequency of ~70 kHz, and a spring constant of ~1 N/m were used. The tapping condition was achieved by setting the cantilever drive frequency to be slightly off of its resonant frequency (~0.05%) and by keeping the set-point amplitude (~6.7 nm) to be ~95.7% of the free amplitude (~7 nm) for imaging in the attractive interaction regimes.[48,69,70] For returning to the same BCP nanodomain areas for repeated imaging, surface defects such as a small dust particle trapped in the ultrathin BCP film were used as a reference to find the original BCP areas of the same fingerprint patterns. The surface coverage of proteins at each time point was determined from the AFM topography images by using the bearing analysis toolset in Bruker AFM software. Adsorption kinetic data were fitted by using curve fitting toolsets available in OriginLab software.

RESULTS AND DISCUSSION

Time Lapse Tracking of IgG Adsorption on the BCP: Single Protein Level Imaging and Kinetics. We have carried out time-lapse AFM imaging of the same PS-*b*-PMMA nanodomain areas exposed to IgG solution and repetitively tracked particular protein molecules of interest over time on the BCP. Representative AFM topography data acquired using this method are presented in Figure 1A where panels i–v mark different states of IgG adsorption and assembly over time on the BCP surface. The repeating stripes in the AFM images are the PS and PMMA nanodomains on the underlying substrate whose nanodomain periodicity is 45 nm (PS to PS distance). The very early adsorption stage of IgG is characterized by a relatively small number of individual protein molecules adsorbing onto available PS nanodomain regions of the BCP in a scattered fashion, as observed in AFM topography panel i. Each IgG molecule can be easily identified as a sphere-shaped object of ~15 nm in diameter against the underlying fingerprint patterns of the BCP nanodomains. As more IgG molecules are adsorbed over time, the surface assembly of IgG in AFM panel ii yielded a line trace of scarcely adsorbed IgG beads on the PS nanodomains, mimicking a sparsely strung strand of IgG beads lying on a PS nanostrip. With further increased adsorption time, more IgG molecules packed into the PS nanodomains as shown in AFM panel iii.

When continuous IgG adsorption reached the stage beyond the line-up in panel iii, further adsorption of IgG molecules led

https://doi.org/10.1021/acs.langmuir.1c02710
Langmuir 2022, 38, 1458–1470

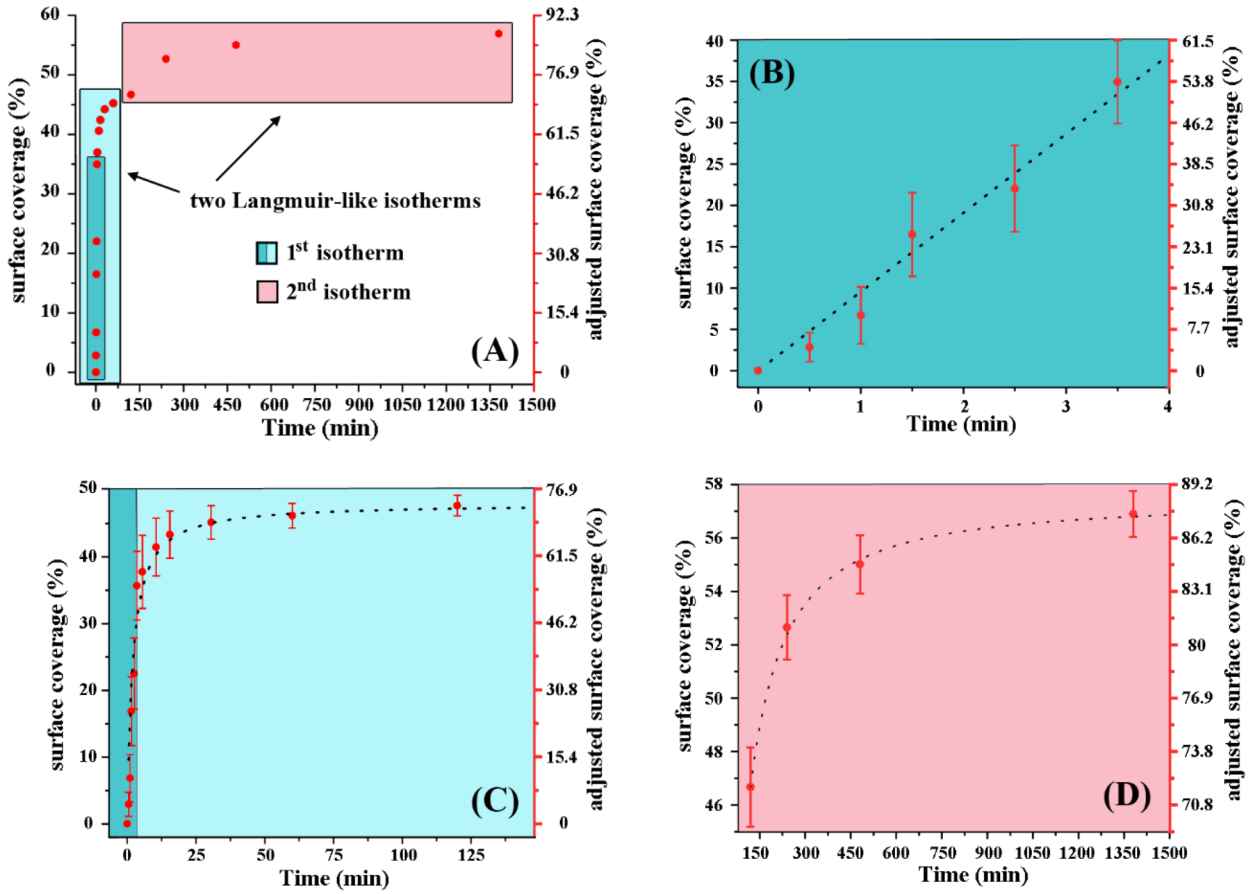

Figure 2. (A) Different adsorption regimes of the time-dependent IgG coverage data on PS-*b*-PMMA are displayed. On the nanoscale, chemically alternating BCP surface, IgG exhibits a unique adsorption kinetic feature exhibiting two Langmuir-like adsorption isotherms. The left (right) vertical axis shown in percent surface coverage (adjusted percent surface coverage) indicates the percent protein surface coverage calculated with respect to the total available surface area on the BCP including the IgG-free PMMA regions (with respect to only the PS nanodomain areas). (B–D) The very early stage data indicated inside the darker blue box in A are shown in B. The first Langmuir-like isotherm segment is shown in C that includes the data points inside the linear (darker blue box) and plateau (lighter blue box) regimes. The second Langmuir-like isotherm segment is presented in D. Dotted lines in all plots are the Hill–Langmuir fits for the data points. Each data point in the adsorption isotherm plot corresponds to IgG surface coverage averaged over 20 different, 2 μm × 2 μm scan areas on the BCP.

to the development of PS nanodomain sections with mixed IgG population of lone as well as paired IgG molecules along the short nanodomain axis. This assembly behavior is displayed in AFM panel iv. PS nanodomain areas occupied by lone (and paired) IgG molecules along the short nanodomain axis are herein referred to as a single (and double) file. As the topography data in Figure 1A are intended to show the overall rather than detailed views of adsorbed IgG molecules covering a relatively large substrate area of the BCP, the exact adsorption processes of individual proteins leading up to the single- and double-file IgG assembly on the PS nanodomains cannot be discerned from these lower magnification images. The biomolecular level description of the IgG surface adsorption and assembly characteristics will be discussed later in this paper using higher magnification AFM data. With more extended IgG adsorption time, all PS nanodomains eventually became fully saturated with IgG molecules adsorbed in a double file. This final stage is shown in AFM panel v. Due to the size of the IgG protein relative to the nanodomain periodicity as well as the exclusive adsorption preference of IgG to PS, the fully saturated assembly of double file IgG molecules on PS in AFM panel v corresponds to the highest, single-layer packing state of IgG permitted on the BCP.

The measured IgG coverage on the PS-*b*-PMMA nanodomain surface is displayed as a function of adsorption time in Figure 1B. Each data point and its error bar in the plot were determined by averaging over 20 independent, 2 μm × 2 μm surface areas after repeatedly tracking the same BCP locations at 15 different time points up to 24 h. The IgG surface coverage shown on the left vertical axis was calculated based on the total BCP surface available to the protein including the protein-covered PS as well as the bare PMMA nanodomains. In addition, adjusted surface coverage was shown in the right vertical axis to reflect the IgG surface coverage with respect to only the surface area of IgG-preferred PS nanodomains. When considering the PS volume fraction of 0.75 in the BCP for a volume-to-area scaling relationship, the BCP nanotemplate presents 65% of PS and 35% of PMMA on its surface. Accordingly, the adjusted surface coverage in Figure 1B corresponds to the footprint taken up by IgG on the BCP if the total available PS nanodomain area is solely considered. The IgG adsorption plot tracked for the same PS-*b*-PMMA areas reveals IgG saturation coverage to be approximately 55% of the total BCP surface and 90% of all available PS nanodomains on the surface. To describe the time-dependent IgG adsorption profile in Figure 1B, we will refer to the trend of an initial,

https://doi.org/10.1021/acs.langmuir.1c02710
Langmuir 2022, 38, 1458–1470

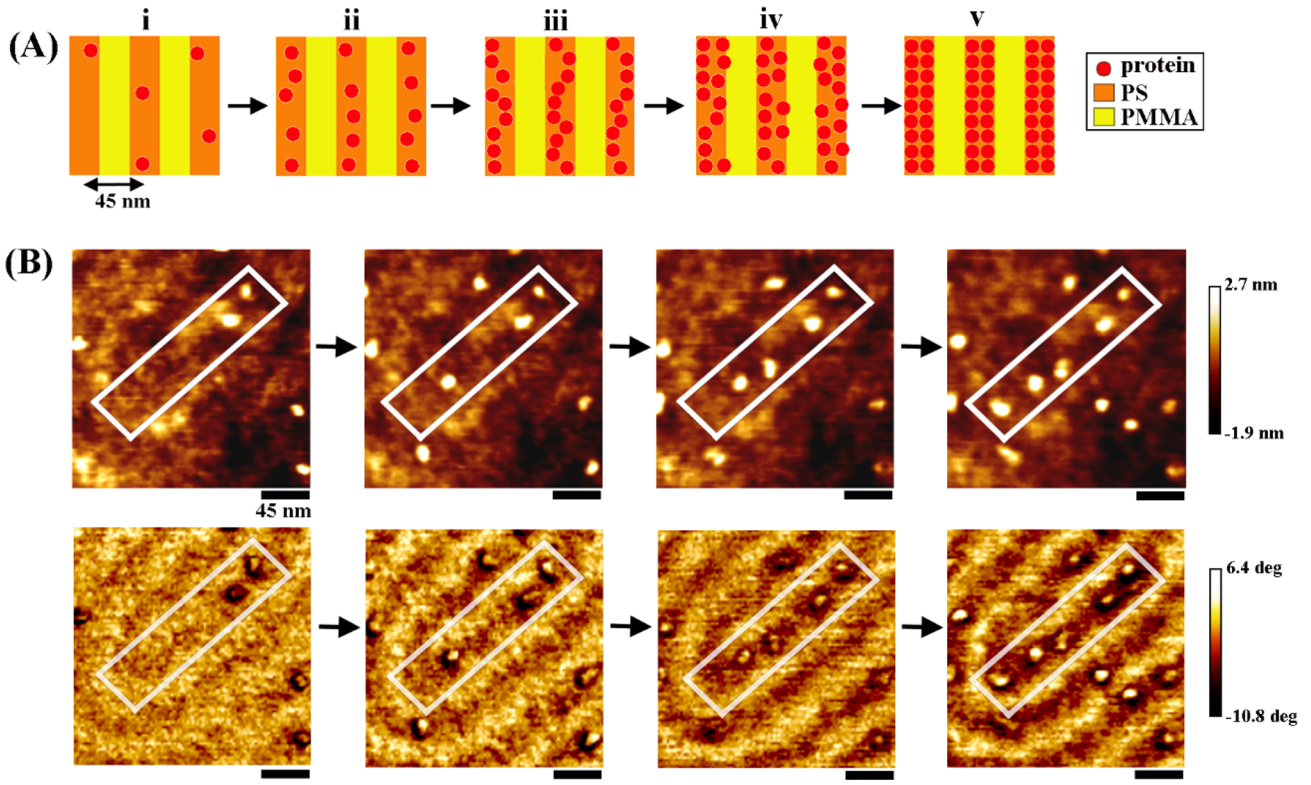

Figure 3. (A) Schematic illustrations depicting the five stages of IgG adsorption identified over time on the BCP surface. They are termed as (i) scattered, (ii) scattered to single file, (iii) single file, (iv) single to double file, and (v) double file states. (B) Representative AFM topography (top row) and phase (bottom row) images of the same BCP area tracked for the very early IgG adsorption stage. The series of AFM data reveal detailed, single biomolecular level snapshots of adsorption substages transitioning over time from (i) scattered to (ii) scattered to single file on the PS nanodomain. White boxes are inserted in the time-lapse AFM frames to guide the eye for finding the same PS nanodomain area. All scale bars shown are 45 nm. All substage panels in B correspond to the very early regime, linearly increasing portion of the adsorption curve in Figure 2A.

linearly increasing followed by a later plateauing surface coverage as a "Langmuir-like" isotherm. Although the general shape of the IgG adsorption curve in Figure 1B may resemble the well-studied isotherm curves in gas and colloid adsorption,[71] it is worthwhile to note that protein adsorption kinetics cannot be described simply by using the same assumptions made in a Langmuir isotherm. This is because additional factors such as reversibility in adsorption, post-adsorption protein conformation change, and postadsorption protein diffusion on the surface can play a significant roles in protein adsorption.[3,72] Indeed, a careful look at the IgG adsorption plot in Figure 1B interestingly reveals two distinct Langmuir-like segments from the IgG adsorption on the nanoscale PS-*b*-PMMA surface, although the IgG adsorption on the BCP over time displays Langmuir-like behaviors overall.

Unique IgG Adsorption Kinetics on the BCP Nanodomain: (1) Two Langmuir-like Segments. The two Langmuir-like curve segments observed from IgG adsorption on the nanoscale polymer surface are clearly marked as the first (blue box) and second (red box) isotherm regions in Figure 2A. Zoomed-in curves for various adsorption time regimes in Figure 2A are subsequently displayed in Figure 2B–D. The graphs in Figure 2B,C together mark the first Langmuir-like isotherm segment. The early stage adsorption profile in Figure 2B indicates that IgG molecules accumulate linearly over time on the BCP surface. The early stage data also show that the linearly increasing adsorption trend continues until IgG covers ~35% of the total BCP (~55% of the available PS nanodomain) area. This IgG surface coverage is reached rapidly within several minutes on the BCP. To better facilitate the ensuing discussions of correlating given surface assembly states of IgG to various regimes in the adsorption plot, the pertinent isotherm curve regions in Figure 1B are denoted by the time-corresponding topographic panels of i–v in Figure 1A. When correlating to the AFM topographic data in Figure 1A, the early stage adsorption plot encompasses topographic stages of i and ii. Following this linear regime, IgG surface coverage increases slowly with time and approaches a plateau regime, as displayed in Figure 2C. The saturation IgG coverage of the first Langmuir-like isotherm is determined to be ~45% of the total BCP (~70% of the available PS nanodomain) area. The IgG assembly state on the BCP at this kinetic regime corresponds to AFM panel iii in Figure 1A. Considering the AFM panels and adsorption plots in Figures 1 and 2 together, the first isotherm segment boxed in blue is determined to be associated with the initial built-up (early linear regime) and subsequent biomolecule organization (later plateau regime) into forming a single file IgG line on the PS nanodomain of the BCP along the long nanodomain axis direction. It was also noticed that the adjusted coverage of IgG at saturation for the single line formation is higher than the expected 50% of the total available PS nanodomain area. This may be related to the observation that IgG molecules in the single line tended to adsorb slightly staggered in a zigzag fashion rather than a straight line with no kinks. It is likely that the staggered rather than straight configuration enables more IgG molecules to adsorb on the surface during the single file assembly.

https://doi.org/10.1021/acs.langmuir.1c02710
Langmuir 2022, 38, 1458–1470

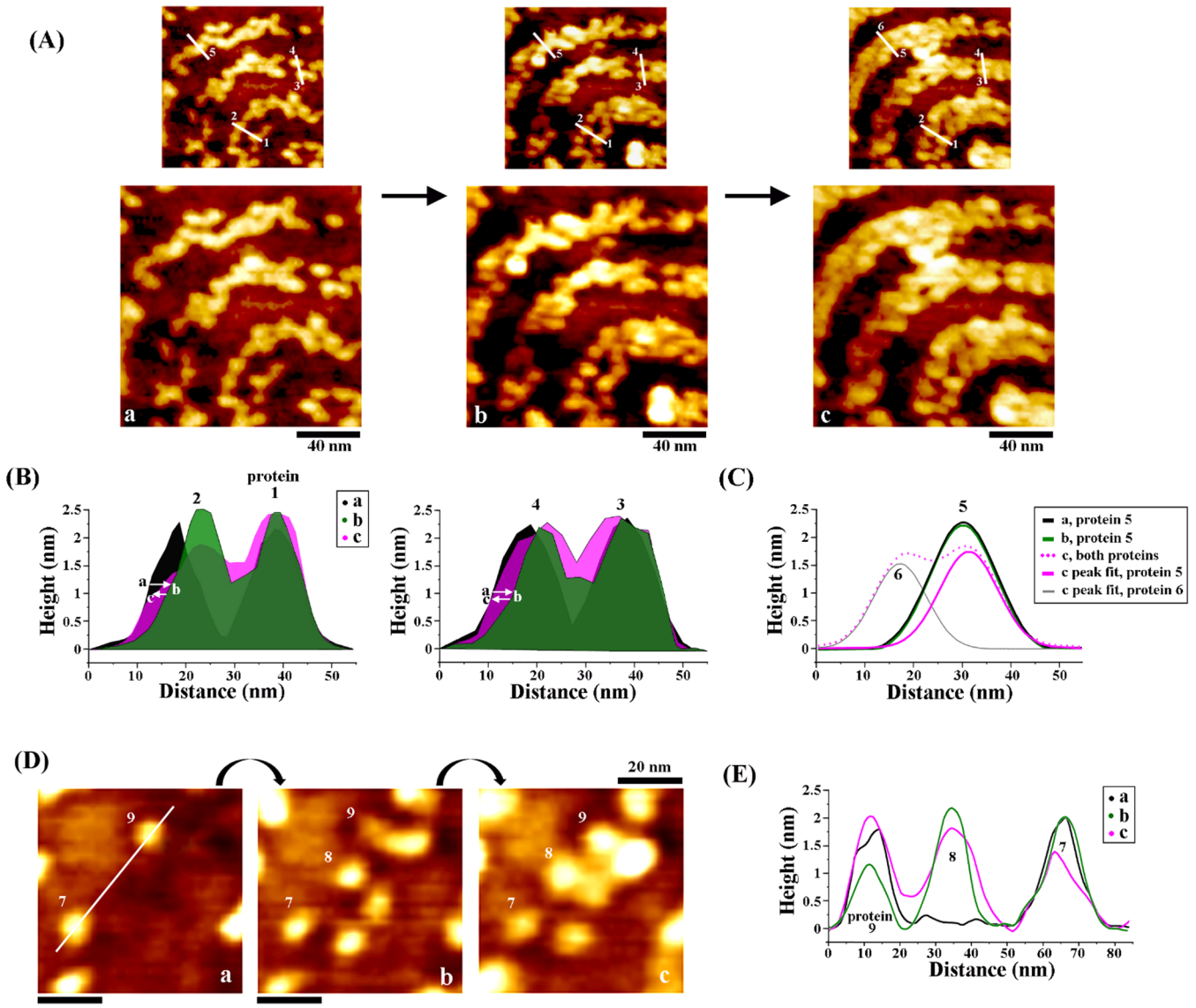

Figure 4. (A) High resolution AFM topography images in a through c display IgG adsorption stages evolving from (iv) single to double file to (v) double file states. The white lines across the numbered proteins, shown in the smaller panels on top of each topography image, specify the sources of the line analysis results presented in B and C. All scale bars shown are 40 nm. (B) For the paired sets of labeled proteins 1−2 and 3−4, line measurements along the short nanodomain axis direction are provided in the left and right plots, respectively. The black, green, and pink traces belong to AFM frames a, b, and c, respectively, and they show the changes in the height and width profiles of the same protein pairs over time. For both pairs of proteins 1−2 and 3−4, the total surface footprint of the paired proteins decreased from frame a to frame b (a → b) after which it increased back in frame c (b → c). (C) Height and width profiles of an initially unpaired but later paired case. Proteins 5−6, are also provided. Black, green, and dotted pink graphs correspond to the line traces along the protein(s) in AFM frames a, b, and c, respectively. Solid pink and gray lines are the curve fits of proteins 5 and 6, respectively, after pairing off in frame c. (D and E) High resolution AFM topography panels in D display the time lapse topography data of a BCP area used for the line analysis along the long nanodomain axis direction shown in E. Changes in the height and width of several adjacently located proteins, proteins 7−9, were analyzed in the long nanodomain direction. The black, green, and pink graphs in E correspond to the line traces in AFM frames a, b, and c, respectively, that were taken through the same set of proteins. All scale bars shown are 20 nm.

IgG adsorption behaviors on the BCP past the first isotherm regime are shown in Figure 2D. The time associated with the initial increase and level-off in the second Langmuir-like adsorption isotherm is much longer (∼1400 min) than that of the first isotherm (∼100 min). The saturation coverage for the second Langmuir-like adsorption isotherm turns out to be ∼55% of the total BCP (∼90% of all available PS nanodomain) surface. The initial rising and later plateauing IgG coverage over time in the second isotherm regimes are associated with the IgG surface assembly state shown in the topography panel of iv and v in Figure 1A, respectively. The correlated outcomes of the topography and kinetic data together indicate that the second isotherm may be attributed to the initial formation of paired IgG molecules on the PS nanodomains along the short nanodomain axis. This subsequently leads to tight packing of IgG molecules in double file lines along the long nanodomain axis and eventually develops into the assembly state of double filed IgG molecules uniformly covering all available PS nanodomains. Unlike the single file IgG assembly in the first isotherm, many more IgG molecules, including those already

https://doi.org/10.1021/acs.langmuir.1c02710
Langmuir 2022, 38, 1458−1470

formed into a single file line, need to cooperatively redistribute to accommodate as many IgG molecules as possible on the surface. This may explain the extended time span associated with the second Langmuir-like isotherm segment relative to the first segment.

IgG Adsorption Pathways Revealed on the BCP Nanodomain: Single to Double File Assembly. The experimental outcomes in Figure 1A indicate that the tight packing geometry of IgG molecules on the BCP was achieved by the formation of a single file IgG line followed by the second line of IgG molecules on the PS nanodomains. In order to gather more conclusive topographic evidence and to better understand the transitions between different segments in the IgG adsorption curve, IgG assembly and packing states on the BCP surface were carefully examined by performing high resolution AFM imaging and resolving single biomolecule level adsorption behaviors corresponding to different isotherm segments. Various adsorption stages and substages were then revealed in AFM topographic data.

The schematic illustrations in Figure 3A depict the IgG arrangements on the BCP nanodomains in various stages of the first (i−iii) and second (iv and v) isotherm segments. We descriptively term the five IgG adsorption regimes as the state of (i) scattered, (ii) scattered to single file, (iii) single file, (iv) single to double file, and (v) double file adsorption on the BCP and will refer to them accordingly for describing the data herein. First, the time-dependent IgG adsorption belonging to the first isotherm segment was tracked and adsorption substeps were scrutinized over time to attain direct experimental evidence for the formation of a single file IgG line on a PS nanodomain. The series of high resolution AFM topography panels in Figure 3B display such substeps existing between the (i) scattered and (iii) single file states. When the accumulation trend of IgG molecules on a PS nanodomain inside the white box area in Figure 3B were tracked over time, IgG adsorption evolved to form a loosely strung single file IgG line in the last frame. The 45 nm periodicity of the BCP nanotemplates provides enough room for two IgG molecules to adsorb side by side along the short axis of the PS nanodomain.[26,31] However, the time lapse tracking data serves as direct evolutionary proof that IgG molecules first assemble in a single file line along the nanodomain long axis, rather than forming paired IgG molecules along the short nanodomain axis first. The topographic substages in Figure 3B are associated with the very early adsorption regime of the first Langmuir-like segment, showing a rapid and linear increase in IgG surface coverage over time. Hence, the high resolution AFM series presented in Figure 3B provide step-by-step biomolecular-level snapshots of the IgG adsorption events taking place on the BCP surface during the linearly increasing portion of the adsorption plot in Figure 2A.

Understanding IgG Assembly via Line Analysis along the Short Nanodomain Axis. The subsequent adsorption stages beyond the first linear regime were also examined at the single biomolecular level. Figure 4 summarizes the time lapse topography images and line analysis traces corresponding to these later times of IgG adsorption. The changes in the width and height of each IgG molecule for the (iii) single file through (v) double file states were determined. Postadsorption processes such as the protein's conformational rearrangements and two-dimensional (2D) translations on the surface were examined. The leftmost frame in Figure 4A shows a transition state of single to double file IgG assembly on PS nanodomains. IgG molecules in some parts have not been paired up yet with another IgG along the nanodomain short axis. In addition, for those areas of double file IgG assembly, a noticeable gap exists between the paired protein molecules which appears as clearly separated, two lines of IgG molecules.

Figure 4B,C are the line analysis profiles taken along the white lines inserted in Figure 4A. The line analyses were performed along the short nanodomain axis by tracking the six proteins numbered as 1−6 in the topography frames of a through c in Figure 4A. The width and height profiles of the paired proteins, 1−2 and 3−4, tracked over time are provided in Figure 4B. The black, green, and pink traces in Figure 4B correspond to the line analysis results from each of these protein pairs as tracked in the AFM frames of a, b, and c, respectively. The gap between the paired proteins of 1 and 2 in AFM frame a was measured to be roughly 10 nm at the full width at half-maximum (fwhm). A similar separation of 10 nm was observed on a neighboring PS nanodomain from the paired proteins of 3 and 4 in AFM frame a. These outcomes suggest that two IgG molecules in the double file line assembly initially prefer to adsorb away from the adsorption partner, on either side of a PS nanostrip as close as possible to the chemical interfaces defined by the alternating PS and PMMA nanodomains. Similar protein adsorption characteristics favoring chemical interfacial regions have been reported in previous studies.[29,31,39] The different chemical environments in the PS:PMMA interfacial regions on the BCP may better satisfy varying interaction needs for the different amino acid moieties on the protein's exterior surface (see Figure S2 in the Supporting Information for IgG, Protein Data Bank ID 1IGT), especially when the periodic length scale of such interfaces is comparable to the single protein dimension. With increasing adsorption time in frames b and c of Figure 4B, the separation distance between the paired proteins was reduced. The green traces in Figure 4B are obtained from the line analysis results of AFM panel *b* from the same two protein pairs. The paired proteins migrated toward each other over time to a separation distance of ∼5 nm at the fwhm. With further transition to AFM frame c, the paired proteins fully closed the gap between them at the fwhm as seen in the pink trace in Figure 4B. Furthermore, the tendency for an increase in overall surface footprints of the protein pairs over time is also evidenced in the pink line traces in Figure 4B for proteins 1−4.

Changes pertaining to an initially unpaired protein are presented in Figure 4C. The line profile of protein 5, adsorbed by itself without an adsorption partner on the PS short nanodomain axis in AFM frame a, is presented in Figure 4C as a black graph. Transitioning to AFM frame b where the protein still remains alone, no significant change was observed in its line analysis profile traced in green. The width of protein 5 without an adsorption partner was measured to be about 20% larger at the fwhm than those of the paired proteins in Figure 4B. This reflects a greater degree of protein chain spreading possible on the PS nanostrip for unpaired proteins relative to paired IgG molecules. This tendency is further evidenced by protein 5 in AFM frame c which underwent substantial changes in its line profile after a new protein, protein 6, occupied the adjacent space. The line profile spanning the two proteins is displayed in dashed pink in Figure 4C. The deconvoluted curve fits are shown in solid pink for protein 5 and gray for protein 6. Upon pairing up, the width of protein 5 in frame c decreased to ∼80% of its unpaired widths in frames a and b. For considering a possible influence from tip

https://doi.org/10.1021/acs.langmuir.1c02710
Langmuir 2022, 38, 1458−1470

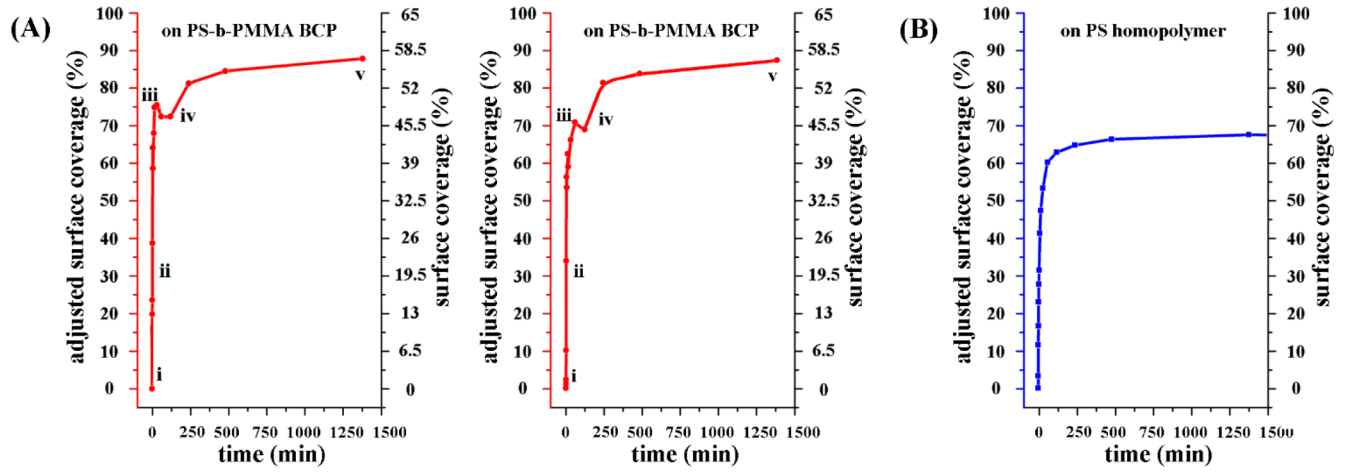

Figure 5. (A) Examples of locally analyzed protein adsorption isotherms on PS-*b*-PMMA showing time-dependent IgG coverage measured from single locations of 2 μm × 2 μm in size. The locally examined IgG adsorption plots on the BCP clearly exhibit an undulating, nonmonotonic segment, i.e. decreasing, and then reincreasing IgG coverage over time. This undulating segment corresponds to the stages of (iii) single file and (iv) single to double file. (B) Representative, locally analyzed adsorption plot obtained from the PS homopolymer surface. Unlike the PS-*b*-PMMA case, IgG surface coverage on the macroscopic, chemically uniform surface shows an adsorption curve profile that continuously increases before flattening out over time.

broadening in AFM measurements, there are different methods such as spherical, Garcia, and step-like models.[73−75] Yet, this inherent convolution effect is not trivial to fully account for or to completely remove from AFM data analysis, especially when imaging proteins on a nanoscale polymer surface. However, it is not likely that the unique IgG adsorption trends discussed in this paper are due to tip broadening. This is because, regardless of whether the protein is paired or unpaired, its overall feature dimension (R) is still roughly on the same order as the tip radius (r). This imposes a similar level of tip convolution effect across all data points and samples in our measurements as a case for $R \approx r$ if the abovementioned models are to be considered. In addition, by conducting a control experiment on a PS homopolymer surface, we rule out any potential tip effect on the distinct trends in the IgG adsorption isotherm on the BCP. The control experiments carried out on PS homopolymer will be discussed later in this paper.

Understanding IgG Assembly via Line Analysis along the Long Nanodomain Axis. We have subsequently examined IgG packing behaviors on the BCP along the long axis of the PS nanodomain. Similar line analyses were performed on a group of adjacent proteins, proteins 7 through 9, along the long nanodomain axis, as seen in the AFM topography series in Figure 4D. The protein width and height profiles tracked over time are then provided in Figure 4E. The surface packing trends of the IgG proteins along the long nanodomain axis direction were similar to what were discussed previously for those along the short nanodomain axis. Proteins 7 and 9 migrated toward one another over time and reduced the gaps between them to accommodate the later arriving protein 8. Compared to the short nanodomain axis results, the effects of protein migration and chain rearrangements were not as pronounced in the line analysis results along the long nanodomain axis. This is likely due to the fact that, in IgG assembly, a higher degree of chemical constraints is imposed by the inherent chemical property of the BCP surface in the short relative to long nanodomain direction. The presence of the IgG-unfavored PMMA nanodomains on either side of a PS nanodomain along the short nanodomain axis may force more pronounced chain rearrangement and 2D translation of the adsorbed proteins. Comparatively speaking, IgG molecules encounter only the favored PS block in the long nanodomain axis direction. With no chemical constraints imposed by the IgG-unfavored PMMA in this direction, protein ordering can be more relaxed over time along the long nanodomain axis.

Unique IgG Adsorption Kinetics on the BCP Nanodomain: (2) Nonmonotonic Regime. Another interesting phenomenon that was observed from the single biomolecular level investigation of the time-dependent IgG adsorption onto the PS-*b*-PMMA surface pertains to the surface footprint of adsorbed protein pairs. According to the evolution in the surface footprint of the protein pairs marked as a → b → c in Figure 4B, the IgG surface footprint decreased (a → b) after which it increased back (b → c) with time. Hence, our single biomolecular level results suggest that the IgG adsorption isotherm on the BCP surface should yield a nonmonotonic segment in which IgG surface coverage undulates over time, i.e. increasing, then decreasing, and finally increasing back over time. However, this trend is not clearly manifested in the adsorption kinetic plot in Figure 2. Although a regime with constant IgG surface coverage over time, i.e. first plateau region, exists before it increases with time at the start of the second isotherm, the expected trend of a downward trajectory in surface coverage followed by an upward recovery over time is not observed in Figure 2.

The adsorption plot in Figure 2 was produced by averaging data from many PS-*b*-PMMA locations to have the total analysis area of ∼100 μm^2. Hypothesizing that the anticipated undulating segment in the adsorption plot may be better identified from locally constructed adsorption curves than the more global area-averaged data, IgG adsorption data from single 2 μm × 2 μm locations were investigated. Two exemplar, local IgG adsorption curves are presented in Figure 5A. The plots in Figure 5A clearly capture a downward dipping followed by upward rising trend over time, consistent with the line analysis outcomes summarized in Figure 4. Eight out of 20 independently analyzed BCP locations of 2 μm × 2 μm in size exhibited a clear "undulating" segment in their adsorption plots as shown in Figure 5A. Additional data obtained by repeating the experiments on an entirely new BCP sample to confirm the

https://doi.org/10.1021/acs.langmuir.1c02710
Langmuir 2022, 38, 1458−1470

undulating trend are also provided in Figure S3 in the Supporting Information. When correlating to the topographic data, the undulating segment of the adsorption plot spanned over the IgG adsorption stages of (iii) single file and (iv) single to double file transition. The other 12 locations displayed a curve profile with no undulating segment similar to Figure 2A. The results discussed here serve as other evidence emphasizing the important fact that protein adsorption behaviors and kinetics cannot be thoroughly understood by solely relying on global, ensemble-averaged data. The experimental outcomes also underscore that, for a comprehensive understanding of protein adsorption, it is critical to determine local, single protein adsorption behaviors and kinetics as they can exhibit much different characteristics than global, ensemble-averaged cases.

Origin of the Two Unique Features in IgG Adsorption on the BCP Nanodomain. Several cases of nonmonotonic adsorption kinetic curves have been previously accounted for in the literature.[34,35,61,62,76] For example, overshooting kinetic behaviors observed in some multicomponent protein adsorption studies were triggered by reconfiguration of a fast diffusing, initially arriving protein species to reduce its surface footprint over time due to the space limitation caused by its replacement by a slower, later arriving protein species.[35,76] Other examples include kinetic overshoots observed from the case of lysozyme adsorption onto a quartz surface[61] as well as from the case of a high concentration (tens of mg/mL) of lysozyme delivered to a hexadecyltrichlorosilane monolayer surface at a relatively large flow rate.[62] Kinetic overshoots were also reported in a study of β-lactoglobulin adsorption onto a glass surface.[34] Direct evidence for single biomolecular level protein adsorption events could not be attained by the experimental techniques employed in these previous studies such as total internal reflectance fluorescence (TIRF), reflectometry, and supercritical angle fluorescence. Hence, the origin of kinetic overshoots had to be either inferred from ensemble-averaged, indirect optical signals obtained from fluorophores tagged onto proteins or deduced from fitted data by applying plausible adsorption models. Moreover, all of these previous cases pertain to adsorption taking place on macroscopic, chemically uniform surfaces. The IgG adsorption isotherm on the BCP identified in the present study are distinct from those found in the above-mentioned studies reporting a single Langmuir-like segment, as discussed earlier. The existence of multiple Langmuir-like isotherm segments as encountered in our present BCP nanodomain work has not been seen from single component protein adsorption onto bulk scale, chemically uniform surfaces.

Compared to the low protein concentration (a few tenths of μg/mL) employed in our study, the overshooting behaviors in the previous works[42−44,49,50] were observed at a much higher bulk protein concentration by at least 2 orders of magnitude. Also, considering that the surfaces in these previous studies were chemically and structurally the same everywhere, the kinetic overshoots reported earlier were likely dictated by protein−protein interactions rather than protein−surface interactions.[34,61,62] In contrast, the experimental condition of surface coverage up to a monolayer employed in the present study is optimized for examining protein−surface interactions. With the nature of dominant protein interactions being entirely different, the existing explanations in the previous works cannot best represent the biomolecular origins of the two unique features in the IgG adsorption isotherm observed on the BCP surface. Rather, by linking the distinct adsorption kinetic segments to the directly visualized individual adsorption events at the single biomolecule level, we determine that the cause of the nonmonotonic adsorption kinetic regimes in our study is strongly driven by the BCP surface and the unique kinetic behaviors of IgG adsorption on the BCP originate from the distinctive spatial and chemical constraints imposed by the underlying PS-*b*-PMMA surface.

IgG Adsorption Mechanisms and Interaction Forces at Play on the BCP Nanodomain. Correlated to the time-tracked, biomolecular level topographic evidence, the unique adsorption kinetic features of the IgG adsorption on the BCP nanodomain are attributed to the adsorption pathway of single to double file assembly adopted by the protein molecules on the BCP surface. It is intriguing to find that, during the IgG adsorption onto the BCP, the single to double file assembly is preferred rather than other pathways such as a case of double file (protein pair formation along the short nanodomain axis first) to its extension (building rows of paired protein molecules along the PS nanostrip). This may be explained as the case of single to double file assembly being the most energetically favored pathway overall, although different protein interaction forces may play a main role at different adsorption stages. In the initial state of single file IgG adsorption, the repulsion of the same charged protein molecules can be best minimized via IgG distribution along the long rather than the short nanodomain axis. With the nanodomain spacing along the BCP's short axis reaching that of the protein dimension, the potential energy penalty due to large electrostatic repulsion between two like-charged proteins will be particularly high for the scenario of forming a double file first. Beyond the initial single file adsorption, additional IgG adsorption from the bulk solution will require an adsorption pathway that produces overall energy gain despite the inevitable increase in electrostatic repulsions between the like-charged protein molecules. Such overall entropic energy gain is possible by having more IgG adsorption and 2D packing on the hydrophobic PS areas of the BCP via the single to double file pathway since more water molecules are released from the PS surface into the bulk solution with more adsorbed IgG.[36]

In all stages of the IgG adsorption, hydrophobic interactions between PS and the protein play a persistently important role. IgG molecules have a tendency to interact solely with the more hydrophobic block of PS on the BCP and adsorb exclusively on the PS area. The energetic interplay of the hydrophobic interaction and electrostatic repulsion may explain why two IgG molecules paired up along the short nanodomain axis are initially found with a noticeable gap between them in Figure 4, while staying as close as possible to the PS:PMMA chemical interfacial regions on either side of a given PS nanodomain. Additional proteins newly adsorbing from the bulk solution will favor the PS region close to the PS:PMMA interface for initial landing to minimize electrostatic repulsion between the proteins. Already surface-bound IgG molecules will then migrate toward the center of the PS nanodomains which is more hydrophobic than the region close to the PS:PMMA interface. The postadsorption 2D translation of the proteins on the surface also enable more IgG adsorption, hence the entropic energy gain as discussed earlier. Together, this explains why this separation between any paired (or neighboring) proteins along the short (or long) nanodomain axis closes in over time, eventually leading to tight surface-

https://doi.org/10.1021/acs.langmuir.1c02710
Langmuir 2022, 38, 1458−1470

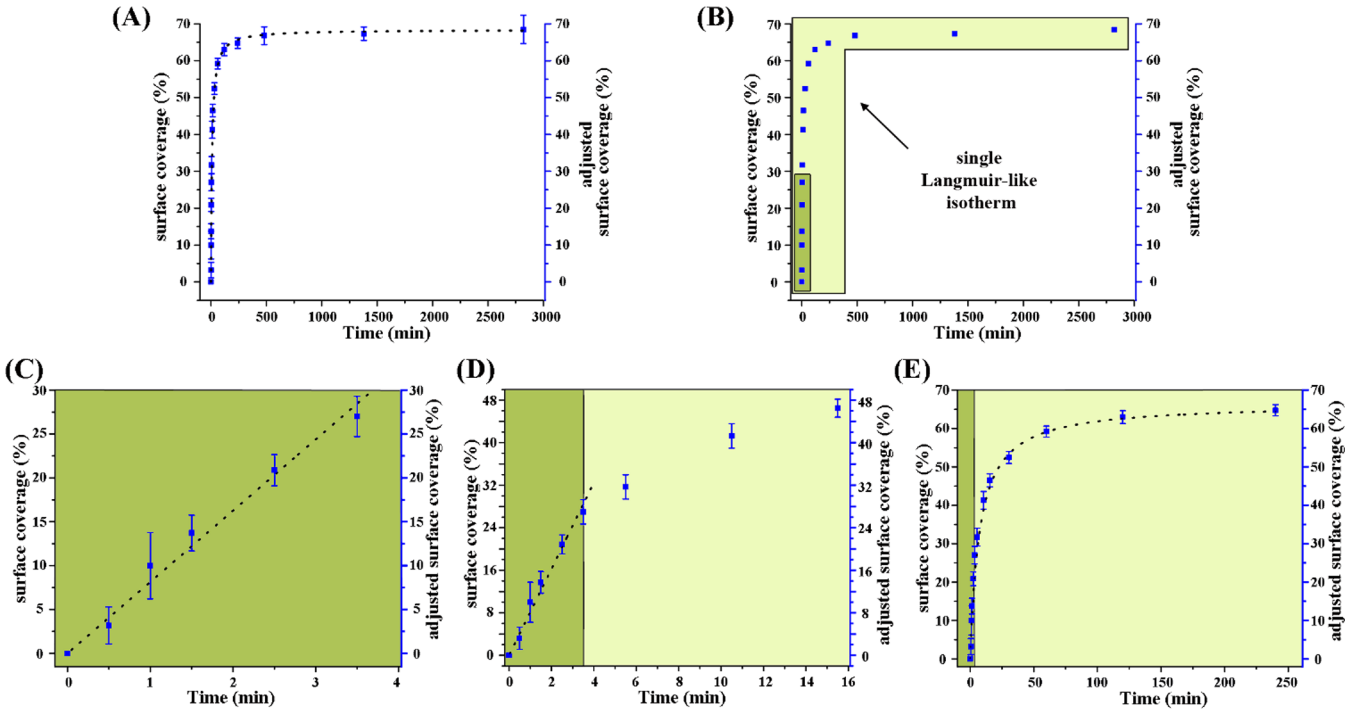

Figure 6. (A) Adsorption kinetic plot constructed by area-averaging IgG coverage from 20 independent areas of 2 μm × 2 μm in size on a PS homopolymer surface over time. The curve displays a single monotonic, Langmuir-like isotherm. (B) The regions of the early time, linearly increasing, as well as the later plateauing regimes are indicated with darker and lighter green shades, respectively. (C–E) The different IgG adsorption segments color-coded in B are shown magnified for clarity. With PS being the sole chemical phase for IgG to adsorb on the PS homopolymer, the surface coverage (left axis) is identical to the adjusted surface coverage (right axis).

packed, IgG molecules forming a double file line on the PS nanodomain until no more sites on PS are available for IgG.

Borrowing the viewpoint of reversible and irreversible adsorption states in existing protein adsorption mechanisms,[5,36,40,41] IgG molecules initially landed on the BCP surface are in a reversible adsorption state and show unoptimized surface packing. They then undergo protein chain rearrangement to optimize IgG surface packing until a fully saturated geometry is achieved on the BCP that mimics a 2D pseudocrystal arrangement. As the protein dwell time on the surface increases, they further go through changes in protein configuration to maximize its interaction with the underlying PS surface and increase its surface footprint. The subsequently established, strong interaction between the protein and the surface makes the protein reach an irreversible adsorption state. Such protein reconfiguration events on the BCP surface are likely to be responsible for the presence of the nonmonotonic segment seen in Figure 5A.

Protein Adsorption on Nanoscale, Chemically Varying vs Macroscale, Chemically Uniform Polymer Surfaces. As discussed earlier, the BCP surface presents well-defined nanoscale surface features with alternating chemical compositions of PS and PMMA. Hence, the assembly and packing of IgG molecules are subject to surface-imposed constraints such as the preferred polymer nanodomain for protein interaction and the chemical interfacial region from the alternating PS and PMMA nanodomains. On top of them, additional confinement is imposed by the width of the preferred nanodomain with respect to the protein size, governing the maximum number of proteins that can be assembled along the short nanodomain axis. The presence and absence of such nanoscale surface-driven factors may result in drastically different, time-dependent packing behaviors and adsorption kinetics of IgG on the nanoscale BCP surface relative to those on chemically homogeneous, macroscopic polymer surfaces. In order to verify this hypothesis that the unique kinetic features of IgG adsorption observed in our study is indeed a nanoscale surface-driven effect, a control experiment was conducted on a PS homopolymer surface. Adsorption plots were subsequently collected by examining the IgG adsorption onto the macroscopic, chemically uniform surface. The time-dependent plot in Figure 5B is a representative graph of IgG surface coverage when analyzed from single 2 μm × 2 μm locations on a PS homopolymer. All 20 locally analyzed adsorption curves on the PS homopolymer exhibited a similar adsorption kinetic profile to the one in Figure 5B. Unlike its counterpart on the nanoscale BCP surface in Figure 5A, the curve profiles of IgG adsorption onto the PS homopolymer showed only one, monotonically increasing, Langmuir-like segment.

As a direct comparison to the results obtained on the BCP in Figure 2, we continued to evaluate IgG adsorption onto the control template of PS homopolymer and obtained an area-averaged adsorption plot from a total analysis area of 100 μm^2. The more globally analyzed data from the macroscopic, chemically uniform PS homopolymer are then summarized in Figure 6A–E. No major differences were found between the more globally (Figure 6A) and locally (Figure 5B) analyzed isotherms for the PS homopolymer case, both of which displayed only a single, monotonic, Langmuir-like segment unlike those of the BCP cases discussed earlier. These results confirm that the existence of two Langmuir-like segments in IgG adsorption isotherms and the appearance of the undulating regimes with nonmonotonic IgG surface coverage

https://doi.org/10.1021/acs.langmuir.1c02710
Langmuir 2022, 38, 1458–1470

over time are associated exclusively with the chemically alternating, nanosized surface features on the BCP surface. Several more differences in the IgG adsorption were noticed from the BCP versus the homopolymer surfaces. When considering the adjusted IgG surface coverage in the very early adsorption, linearly increasing regimes in Figures 2B and 6C, the adsorption rate was found to be much higher on the BCP (~40% after 3 min) relative to the PS homopolymer case (~20% after 3 min). The IgG saturation coverage also differs on the two surface cases. The adjusted protein coverage for the final saturation regime was higher on the BCP (~90%) than on the PS homopolymer (~65%). This indicates that, when using identical protein deposition conditions, the surface density of adsorbed IgG (the number of IgG molecules per given PS area) will be higher on the BCP relative to the homopolymer surface. IgG loading onto a polymer surface, therefore, will be much more effective if a nanoscale, chemically varying BCP surface is used instead of a macroscopic, chemically uniform homopolymer surface.

CONCLUSION

We have revealed unique, time-dependent protein adsorption behaviors at the single biomolecule level on the chemically alternating BCP nanodomains of PS-*b*-PMMA. The exact adsorption pathways and kinetics of IgG molecules, eventually yielding a tight surface packed geometry that mimics a 2D pseudocrystal structure, were determined. A distinct adsorption pathway of a single to double file IgG assembly was revealed on BCP. In addition, two unique characteristics of IgG adsorption on the nanoscale BCP surface were identified, i.e., the presence of two Langmuir-like segments and the existence of an undulating, nonmonotonic adsorption regime. The direct experimental proof provided in this study, linking given topological protein assembly states to specific adsorption kinetic regimes, made it possible to ascertain the biomolecular-level origins for many intriguing time-dependent IgG adsorption characteristics on the nanoscale polymer surface that could not be attained before. The distinctive IgG adsorption pathways and kinetics on the BCP surface were driven by the surface effect whose chemically alternating feature sizes on the surface are comparable to the size of the individual protein.

The successfully implemented approach for relating key segments of adsorption kinetic plots to directly visualized, nanoscopic adsorption events on the nanodomain surface is especially valuable considering that such single biomolecule level experimental evidence has been long sought after to verify common assumptions in protein adsorption and to build an entirely new mechanism. Our approach can be also useful for establishing mechanistic understandings of time-dependent protein adsorption behaviors on other biomedically important BCP and protein systems, beyond the model protein and BCP chosen in this study. Furthermore, the overall methodology demonstrated for elucidating time-dependent nanoscale protein adsorption mechanisms and kinetics can be beneficial for the development of advanced biomaterials and miniaturized biodevices based on protein interactions with nanoscale, chemically varying polymer surfaces.

ASSOCIATED CONTENT

Supporting Information

The Supporting Information is available free of charge at https://pubs.acs.org/doi/10.1021/acs.langmuir.1c02710.

Figure S1: AFM phase panel of a clean PS-*b*-PMMA film. Figure S2: Surface of IgG (Protein Data Bank ID 1IGT) mapped for its hydrophobicity as well as surface charge at pH 7.4. Figure S3: Additional IgG adsorption isotherm data obtained by repeating the experiments described in Figure 5 (PDF)

AUTHOR INFORMATION

Corresponding Author

Jong-in Hahm − *Department of Chemistry, Georgetown University, Washington, D.C. 20057, United States;* orcid.org/0000-0003-4395-1669; Email: jh583@georgetown.edu

Authors

David H. Cho − *Department of Chemistry, Georgetown University, Washington, D.C. 20057, United States*

Tian Xie − *Department of Chemistry, Georgetown University, Washington, D.C. 20057, United States*

Patrick J. Mulcahey − *Department of Chemistry, Georgetown University, Washington, D.C. 20057, United States*

Noah P. Kelleher − *Department of Chemistry, Georgetown University, Washington, D.C. 20057, United States*

Complete contact information is available at: https://pubs.acs.org/10.1021/acs.langmuir.1c02710

Notes

The authors declare no competing financial interest.

ACKNOWLEDGMENTS

The authors acknowledge financial support on this work by the National Science Foundation (Award No. CHE1903857) from the Macromolecular, Supramolecular and Nanochemistry Program under the Division of Chemistry.

REFERENCES

(1) Gray, J. J. The Interaction of Proteins with Solid Surfaces. *Curr. Opin. Struct. Biol.* **2004**, *14* (1), 110−115.

(2) Hlady, V.; Buijs, J. Protein Adsorption on Solid Surfaces. *Curr. Opin. Biotechnol.* **1996**, *7* (1), 72−77.

(3) Latour, R. A., Biomaterials: Protein−Surface Interactions. In *Encyclopedia of Biomaterials and Biomedical Engineering*, 2nd ed.; Informa Healthcare: 2008; Vol. *1*, pp 270−284.

(4) Nakanishi, K.; Sakiyama, T.; Imamura, K. On the Adsorption of Proteins on Solid Surfaces, a Common but Very Complicated Phenomenon. *J. Biosci. Bioeng.* **2001**, *91*, 233−244.

(5) Rabe, M.; Verdes, D.; Seeger, S. Understanding Protein Adsorption Phenomena at Solid Surfaces. *Adv. Colloid Interface Sci.* **2011**, *162* (1−2), 87−106.

(6) Szleifer, I. Polymers and Proteins: Interactions at Interfaces. *Curr. Opin. Solid State Mater. Sci.* **1997**, *2* (3), 337−344.

(7) Talapatra, A.; Rouse, R.; Hardiman, G. Protein Microarrays: Challenges and Promises. *Pharmacogenomics* **2002**, *3* (4), 527.

(8) Spillman, S. D.; McEvoy, H. M.; MacCraith, B. D. Fabrication of Substrate-Independent Protein Microarrays Using Polyelectrolyte Scaffolding. *Langmuir* **2009**, *25* (3), 1403−1411.

(9) Cummins, C.; Lundy, R.; Walsh, J. J.; Ponsinet, V.; Fleury, G.; Morris, M. A. Enabling Future Nanomanufacturing through Block Copolymer Self-Assembly: A Review. *Nano Today* **2020**, *35*, 100936.

(10) Bhushan, B.; Schricker, S. R. A Review of Block Copolymer-Based Biomaterials That Control Protein and Cell Interactions. *J. Biomed. Mater. Res., Part A* **2014**, *102* (7), 2467−2480.

(11) Biswas, A.; Shukla, A.; Maiti, P. Biomaterials for Interfacing Cell Imaging and Drug Delivery: An Overview. *Langmuir* **2019**, *35* (38), 12285−12305.

(12) Hahm, J. Functional Polymers in Protein Detection Platforms: Optical, Electrochemical, Electrical, Mass-sensitive, and Magnetic Biosensors. *Sensors* **2011**, *11* (3), 3327−3355.
(13) Hahm, J. Polymeric Surface-Mediated, High-density Nanoassembly of Functional Protein Arrays. *J. Biomed. Nanotechnol.* **2011**, *7* (6), 731−742.
(14) Wang, H.; Akcora, P. Confinement Effect on the Structure and Elasticity of Proteins Interfacing Polymers. *Soft Matter* **2017**, *13*, 1561−1568.
(15) Ulusan, S.; Butun, V.; Banerjee, S.; Erel-Goktepe, I. Biologically Functional Ultrathin Films Made of Zwitterionic Block Copolymer Micelles. *Langmuir* **2019**, *35* (5), 1156−1171.
(16) Li, X.; Wang, M.; Wang, L.; Shi, X.; Xu, Y.; Song, B.; Chen, H. Block Copolymer Modified Surfaces for Conjugation of Biomacromolecules with Control of Quantity and Activity. *Langmuir* **2013**, *29* (4), 1122−1128.
(17) Bates, C. M.; Maher, M. J.; Janes, D. W.; Ellison, C. J.; Willson, C. G. Block Copolymer Lithography. *Macromolecules* **2014**, *47* (1), 2−12.
(18) Bates, F. S.; Fredrickson, G. H. Block Copolymer Thermodynamics - Theory and Experiment. *Annu. Rev. Phys. Chem.* **1990**, *41*, 525−557.
(19) Darling, S. B. Directing the Self-Assembly of Block Copolymers. *Prog. Polym. Sci.* **2007**, *32* (10), 1152−1204.
(20) Fredrickson, G. H.; Bates, F. S. Dynamics of Block Copolymers: Theory and Experiment. *Annu. Rev. Mater. Sci.* **1996**, *26*, 501−550.
(21) Kumar, N.; Parajuli, O.; Hahm, J. Two-dimensionally Self-arranged Protein Nanoarrays on Diblock Copolymer Templates. *J. Phys. Chem. B* **2007**, *111*, 4581−4587.
(22) Song, S.; Milchak, M.; Zhou, H. B.; Lee, T.; Hanscom, M.; Hahm, J. I. Nanoscale Protein Arrays of Rich Morphologies via Self-assembly on Chemically Treated Diblock Copolymer Surfaces. *Nanotechnology* **2013**, *24* (9), 095601.
(23) Cho, D. H.; Xie, T.; Truong, J.; Stoner, A. C.; Hahm, J. Recent Advances towards Single Biomolecule Level Understanding of Protein Adsorption Phenomena Unique to Nanoscale Polymer Surfaces with Chemical Variations. *Nano Res.* **2020**, *13*, 1295−1317.
(24) Malmström, J.; Travas-Sejdic, J. Block Copolymers for Protein Ordering. *J. Appl. Polym. Sci.* **2014**, *131* (14), 40360.
(25) Kollmetz, T.; Monteiro A, I.; Gerrard, J. A.; Malmström, J. Polystyrene-block-Poly(ethylene oxide) Thin Films Fabricated from a Solvent Mixture for the Co-Assembly of Polymers and Proteins. *ACS Omega* **2020**, *5* (41), 26365−26373.
(26) Kumar, N.; Hahm, J. Nanoscale Protein Patterning Using Self-assembled Diblock Copolymers. *Langmuir* **2005**, *21*, 6652−6655.
(27) Kumar, N.; Parajuli, O.; Dorfman, A.; Kipp, D.; Hahm, J. Activity Study of Self-assembled Proteins on Nanoscale Diblock Copolymer Templates. *Langmuir* **2007**, *23*, 7416−7422.
(28) Cho, D. H.; Hahm, J. Protein−Polymer Interaction Characteristics Unique to Nanoscale Interfaces: A Perspective on Recent Insights. *J. Phys. Chem. B* **2021**, *125* (23), 6040−6057.
(29) Kumar, N.; Parajuli, O.; Gupta, A.; Hahm, J. Elucidation of Protein Adsorption Behavior on Polymeric Surfaces: Towards High Density, High Payload, Protein Templates. *Langmuir* **2008**, *24*, 2688−2694.
(30) Parajuli, O.; Gupta, A.; Kumar, N.; Hahm, J. Evaluation of Enzymatic Activity on Nanoscale PS-b-PMMA Diblock Copolymer Domains. *J. Phys. Chem. B* **2007**, *111*, 14022−14027.
(31) Hahm, J. Fundamentals of Nanoscale Polymer-Protein Interactions and Potential Contributions to Solid-state Nanobioarrays. *Langmuir* **2014**, *30*, 9891−9904.
(32) Song, S.; Ravensbergen, K.; Alabanza, A.; Soldin, D.; Hahm, J. Distinct Adsorption Configurations and Self-Assembly Characteristics of Fibrinogen on Chemically Uniform and Alternating Surfaces including Block Copolymer Nanodomains. *ACS Nano* **2014**, *8* (5), 5257−5269.
(33) Xie, T.; Vora, A.; Mulcahey, P. J.; Nanescu, S. E.; Singh, M.; Choi, D. S.; Huang, J. K.; Liu, C.-C.; Sanders, D. P.; Hahm, J. Surface Assembly Configurations and Packing Preferences of Fibrinogen Mediated by the Periodicity and Alignment Control of Block Copolymer Nanodomains. *ACS Nano* **2016**, *10* (8), 7705−7720.
(34) Rabe, M.; Verdes, D.; Rankl, M.; Artus, G. R. J.; Seeger, S. A Comprehensive Study of Concepts and Phenomena of the Non-specific Adsorption of β-Lactoglobulin. *ChemPhysChem* **2007**, *8* (6), 862−872.
(35) Ramsden, J. J. Puzzles and Paradoxes in Protein Adsorption. *Chem. Soc. Rev.* **1995**, *24* (1), 73−78.
(36) Norde, W.; Haynes, C. A., Reversibility and the Mechanism of Protein Adsorption. In *Proteins at Interfaces II*, Horbett, T. A.; Brash, J. L., Eds. American Chemical Society: 1995; Vol. *602*, pp 26−40.
(37) Song, S.; Xie, T.; Ravensbergen, K.; Hahm, J.-i. Ascertaining Effects of Nanoscale Polymeric Interfaces on Competitive Protein Adsorption at the Individual Protein Level. *Nanoscale* **2016**, *8* (6), 3496−3509.
(38) Xie, T.; Chattoraj, J.; Mulcahey, P. J.; Kelleher, N. P.; Del Gado, E.; Hahm, J. Revealing the Principal Attributes of Protein Adsorption on Block Copolymer Surfaces with Direct Experimental Evidence at the Single Protein Level. *Nanoscale* **2018**, *10* (19), 9063−9076.
(39) Lau, K. H. A.; Bang, J.; Kim, D. H.; Knoll, W. Self-Assembly of Protein Nanoarrays on Block Copolymer Templates. *Adv. Funct. Mater.* **2008**, *18* (20), 3148−3157.
(40) Penna, M. J.; Mijajlovic, M.; Biggs, M. J. Molecular-Level Understanding of Protein Adsorption at the Interface between Water and a Strongly Interacting Uncharged Solid Surface. *J. Am. Chem. Soc.* **2014**, *136* (14), 5323−5331.
(41) Ozboyaci, M.; Kokh, D. B.; Corni, S.; Wade, R. C. Modeling and Simulation of Protein−Surface Interactions: Achievements and Challenges. *Q. Rev. Biophys.* **2016**, *49* (e4), 1−45.
(42) Müller, D. J.; Janovjak, H.; Lehto, T.; Kuerschner, L.; Anderson, K. Observing Structure, Function and Assembly of Single Proteins by AFM. *Prog. Biophys. Mol. Biol.* **2002**, *79* (1), 1−43.
(43) Dufrêne, Y. F.; Ando, T.; Garcia, R.; Alsteens, D.; Martinez-Martin, D.; Engel, A.; Gerber, C.; Müller, D. J. Imaging Modes of Atomic Force Microscopy for Application in Molecular and Cell Biology. *Nat. Nanotechnol.* **2017**, *12* (4), 295−307.
(44) Dufrêne, Y. F.; Marchal, T. G.; Rouxhet, P. G. Influence of Substratum Surface Properties on the Organization of Adsorbed Collagen Films: In Situ Characterization by Atomic Force Microscopy. *Langmuir* **1999**, *15* (8), 2871−2878.
(45) Denis, F. A.; Hanarp, P.; Sutherland, D. S.; Gold, J.; Mustin, C.; Rouxhet, P. G.; Dufrêne, Y. F. Protein Adsorption on Model Surfaces with Controlled Nanotopography and Chemistry. *Langmuir* **2002**, *18* (3), 819−828.
(46) Alsteens, D.; Müller, D. J.; Dufrêne, Y. F. Multiparametric Atomic Force Microscopy Imaging of Biomolecular and Cellular Systems. *Acc. Chem. Res.* **2017**, *50* (4), 924−931.
(47) Schön, P.; Görlich, M.; Coenen, M. J. J.; Heus, H. A.; Speller, S. Nonspecific Protein Adsorption at the Single Molecule Level Studied by Atomic Force Microscopy. *Langmuir* **2007**, *23* (20), 9921−9923.
(48) San Paulo, A.; García, R. High-Resolution Imaging of Antibodies by Tapping-Mode Atomic Force Microscopy: Attractive and Repulsive Tip-Sample Interaction Regimes. *Biophys. J.* **2000**, *78* (3), 1599−1605.
(49) Vilhena, J. G.; Dumitru, A. C.; Herruzo, E. T.; Mendieta-Moreno, J. I.; Garcia, R.; Serena, P. A.; Pérez, R. Adsorption Orientations and Immunological Recognition of Antibodies on Graphene. *Nanoscale* **2016**, *8* (27), 13463−13475.
(50) Chen, X.; Davies, M. C.; Roberts, C. J.; Tendler, S. J. B.; Williams, P. M.; Davies, J.; Dawkes, A. C.; Edwards, J. C. Recognition of Protein Adsorption onto Polymer Surfaces by Scanning Force Microscopy and Probe−Surface Adhesion Measurements with Protein-Coated Probes. *Langmuir* **1997**, *13* (15), 4106−4111.
(51) Chen, S.; Roseman, A. M.; Hunter, A. S.; Wood, S. P.; Burston, S. G.; Ranson, N. A.; Clarke, A. R.; Saibil, H. R. Location of a Folding Protein and Shape Changes in GroEL−GroES Complexes Imaged by Cryo-Electron Microscopy. *Nature* **1994**, *371* (6494), 261−264.

https://doi.org/10.1021/acs.langmuir.1c02710
Langmuir 2022, 38, 1458−1470

(52) Zhang, L.; Song, J.; Cavigiolio, G.; Ishida, B. Y.; Zhang, S.; Kane, J. P.; Weisgraber, K. H.; Oda, M. N.; Rye, K.-A.; Pownall, H. J.; Ren, G. Morphology and Structure of Lipoproteins Revealed by an Optimized Negative-Staining Protocol of Electron Microscopy. *J. Lipid Res.* **2011**, *52* (1), 175−184.
(53) Zhang, X.; Zhang, L.; Tong, H.; Peng, B.; Rames, M. J.; Zhang, S.; Ren, G. 3D Structural Fluctuation of IgG1 Antibody Revealed by Individual Particle Electron Tomography. *Sci. Rep.* **2015**, *5*, 9803.
(54) Weisel, J. W.; Phillips, G. N.; Cohen, C. A Model from Electron Microscopy for the Molecular Structure of Fibrinogen and Fibrin. *Nature* **1981**, *289*, 263−267.
(55) Veklich, Y. I.; Gorkun, O. V.; Medved, L. V.; Nieuwenhuizen, W.; Weisel, J. W. Carboxyl-Terminal Portions of the Alpha Chains of Fibrinogen and Fibrin. Localization by Electron Microscopy and the Effects of Isolated Alpha C Fragments on Polymerization. *J. Biol. Chem.* **1993**, *268* (18), 13577−13585.
(56) Thompson, R. F.; Walker, M.; Siebert, C. A.; Muench, S. P.; Ranson, N. A. An Introduction to Sample Preparation and Imaging by Cryo-Electron Microscopy for Structural Biology. *Methods* **2016**, *100*, 3−15.
(57) Hlady, V.; Buijs, J.; Jennissen, H. P. Methods for Studying Protein Adsorption. *Method. Enzymol.* **1999**, *309*, 402−429.
(58) Soteropulos, C. E.; Zurick, K. M.; Bernards, M. T.; Hunt, H. K. Tailoring the Protein Adsorption Properties of Whispering Gallery Mode Optical Biosensors. *Langmuir* **2012**, *28* (44), 15743−15750.
(59) Ramsden, J. J. Experimental Methods for Investigating Protein Adsorption Kinetics at Surfaces. *Q. Rev. Biophys.* **1994**, *27* (1), 41−105.
(60) Bhakta, S. A.; Evans, E.; Benavidez, T. E.; Garcia, C. D. Protein Adsorption onto Nanomaterials for the Development of Biosensors and Analytical Devices: A Review. *Anal. Chim. Acta* **2015**, *872*, 7−25.
(61) Daly, S. M.; Przybycien, T. M.; Tilton, R. D. Coverage-Dependent Orientation of Lysozyme Adsorbed on Silica. *Langmuir* **2003**, *19* (9), 3848−3857.
(62) Wertz, C. F.; Santore, M. M. Adsorption and Reorientation Kinetics of Lysozyme on Hydrophobic Surfaces. *Langmuir* **2002**, *18* (4), 1190−1199.
(63) Chen, Q.; Tang, W.; Wang, D.; Wu, X.; Li, N.; Liu, F. Amplified QCM-D Biosensor for Protein Based on Aptamer-Functionalized Gold Nanoparticles. *Biosens. Bioelectron.* **2010**, *26* (2), 575−579.
(64) Uludag, Y.; Tothill, I. E. Cancer Biomarker Detection in Serum Samples Using Surface Plasmon Resonance and Quartz Crystal Microbalance Sensors with Nanoparticle Signal Amplification. *Anal. Chem.* **2012**, *84* (14), 5898−5904.
(65) Monteiro A, I.; Kollmetz, T.; Musson, D. S.; McGlashan, S. R.; Malmström, J. Polystyrene-block-Polyethylene Oxide Thin Films: In vitro Cytocompatibility and Protein Adsorption Testing. *Biointerphases* **2020**, *15* (1), 011003.
(66) Malmström, J.; Agheli, H.; Kingshott, P.; Sutherland, D. S. Viscoelastic Modeling of Highly Hydrated Laminin Layers at Homogeneous and Nanostructured Surfaces: Quantification of Protein Layer Properties Using QCM-D and SPR. *Langmuir* **2007**, *23* (19), 9760−9768.
(67) Wu, J. G.; Wei, S. C.; Chen, Y.; Chen, J. H.; Luo, S. C. Critical Study of the Recognition between C-Reactive Protein and Surface-Immobilized Phosphorylcholine by Quartz Crystal Microbalance with Dissipation. *Langmuir* **2018**, *34* (3), 943−951.
(68) Delcroix, M. F.; Demoustier-Champagne, S.; Dupont-Gillain, C. C. Quartz Crystal Microbalance Study of Ionic Strength and pH-Dependent Polymer Conformation and Protein Adsorption/Desorption on PAA, PEO, and Mixed PEO/PAA Brushes. *Langmuir* **2014**, *30* (1), 268−277.
(69) García, R.; San Paulo, A. Attractive and Repulsive Tip-Sample Interaction Regimes in Tapping-Mode Atomic Force Microscopy. *Phys. Rev. B* **1999**, *60* (7), 4961−4967.
(70) García, R.; San Paulo, A. Amplitude Curves and Operating Regimes in Dynamic Atomic Force Microscopy. *Ultramicroscopy* **2000**, *82* (1), 79−83.
(71) Butt, H.; Graf, K.; Kappl, M., Adsorption. In *Physics and Chemistry of Interfaces*; Butt, H., Graf, K., Kappl, M., Eds.; John Wiley & Sons, Inc., 2004.
(72) Latour, R. A. The Langmuir Isotherm: A Commonly Applied but Misleading Approach for the Analysis of Protein Adsorption Behavior. *J. Biomed. Mater. Res. Part A* **2015**, *103* (3), 949−958.
(73) Winzer, A. T.; Kraft, C.; Bhushan, S.; Stepanenko, V.; Tessmer, I. Correcting for AFM Tip Induced Topography Convolutions in Protein−DNA Samples. *Ultramicroscopy* **2012**, *121*, 8−15.
(74) Garcia, V. J.; Martinez, L.; Briceno-Valero, J. M.; Schilling, C. H. Dimensional Metrology of Nanometric Spherical Particles Using AFM: 1, Model Development. *Probe Microsc.* **1997**, *1* (1), 107−116.
(75) Ruggeri, F. S.; Šneideris, T.; Vendruscolo, M.; Knowles, T. P. J. Atomic Force Microscopy for Single Molecule Characterisation of Protein Aggregation. *Arch. Biochem. Biophys.* **2019**, *664*, 134−148.
(76) Tremsina, Y. S.; Sevastianov, V. I.; Petrash, S.; Dando, W.; Foster, M. D. Competitive Adsorption of Human Serum Albumin and Gamma-Globulin from a Binary Protein Mixture onto Hexadecyltrichlorosilane Coated Glass. *J. Biomater. Sci. Poly. Ed.* **1998**, *9* (2), 151−161.

https://doi.org/10.1021/acs.langmuir.1c02710
Langmuir 2022, 38, 1458−1470